Carbon fibre–thermoplastic matrix adhesion

L. DI LANDRO, M. PEGORARO
Dipartimento di Chimica Industriale e Ingegneria Chimica "G. Natta", Politecnico di Milano, Milano, Italy

Adhesion between carbon fibres and amorphous thermoplastic matrices with high distortion temperature (polyetherimide and polyethersulphone) is studied. Shear strength at the fibre–matrix interface has been accurately evaluated according to a statistical method based on the measurement of the mean critical fibre length. In the evaluation of critical length, the tensile strength due to the fibre defects, may be accounted for using Weibull's model. On the basis of these and other tests, such as scanning electron microscopy, X-ray photoelectron spectroscopy and punch tool, adhesion is discussed: its prevailing mechanism is attributed to the differential thermal shrinkage of fibre and matrices.

1. Introduction

Evaluation of adhesion between polymeric matrices and reinforcing fibres is of remarkable importance in the study of the mechanical behaviour of composite materials. The fibre–matrix interface is a critical area in determining the composite strength with more or less perfect continuity. The use of high tensile strength fibres, such as carbon fibres, and of thermoplastic matrices having a high distortion temperature, has increasing importance in their application.

This work reports the study of adhesion between carbon fibres and amorphous materials such as polyethersulphone (PES) and polyetherimide (ULTEM). A method for measurement of fibre–matrix adhesion stress (τ_{ad}), already suggested for use with other types of materials was used [1, 2]. On the basis of other tests, the adhesion mechanism is discussed.

2. Relations between adhesion shear stress, critical length and fibre strength

It is known that a reinforcing effect can be obtained only if the volumetric fraction of fibres is higher than a minimum value (V_{min}) [3]. Below this value during a tensile test the fibres break at small elongation without involving failure of the whole composite. In the ideal case, all the fibres, if continuous, are loaded at each point at the same stress. This should cause formation of more fragments.

Let us consider a fibre of length, l, and diameter, d, immersed in a matrix keeping its volumetric fraction lower than V_{min} (Fig. 1). Under axial load the equilibrium equation gives:

$$\tau(\pi d)\mathrm{d}x = (\pi d^2/4)\mathrm{d}\sigma_f \quad (1)$$

and

$$\tau = \frac{d}{4}\frac{\mathrm{d}\sigma_f}{\mathrm{d}x} \quad (2)$$

therefore

$$\sigma_f(x) = \int [4\tau(x)/d]\mathrm{d}x \quad (3)$$

where $\tau(x)$ is the shear stress present at the interface. Stress analysis allows calculation of $\tau(x)$ and $\sigma_f(x)$ at different points of the fibre [3]. For low external loads the values range from a maximum at the fibre end down to zero in the central part of the fibre; vice versa, according to Equation 3, σ_f is zero at the ends and a maximum in the central part (Fig. 2a).

As the external load is increased, τ reaches the yielding shear stress of the matrix (τ_y) beginning at the fibre ends in the case of good adhesion, or reaches the shear limit of adhesion (τ_{ad}) when the latter is lower than the matrix yield shear stress (Fig. 2b).

When the τ limit (τ_l) is reached, a further increase in σ_f and in load is possible, because a larger interfacial area is involved by the shear phenomena (Fig. 2c). The fibre will be subjected to a stress, σ, which linearly increases from the fibre ends towards the centre along the length, $\bar{x}$, where τ is constant (Equation 3) (Fig. 2c, d). Beyond $\bar{x}$ the stress in the fibre is practically constant:

$$\sigma_f = 4\tau_l\bar{x}/d \quad (4)$$

The failure of the fibre occurs when the stress, σ_f reaches the tensile strength (σ_{rf}):

$$\sigma_{rf} = 4\tau_l\bar{x}/d$$

that is

$$\bar{X} = \frac{\sigma_{rf}d}{4\tau_l} \quad (5)$$

This length is defined as the semicritical length ($l_{cr}/2$) [3]. In the case of fibre lengths lower than l_{cr} the tensile strength of the fibre cannot be reached. According to Equation 5, therefore, we set:

$$l_{cr} = \frac{\sigma_{rf}d}{2\tau_l} \quad \text{and} \quad \tau_l = \frac{\sigma_{rf}d}{2l_{cr}} \quad (6)$$

By assuming that the fibre is sufficiently long, the fibre fragmentation will continue until each fragment is reduced to a length $l \leqslant l_{cr}$. When a fragment of length higher than l_{cr} fails, failure can occur at any point of its central part where σ is constant and equal

0022–2461/87 $03.00 + .12

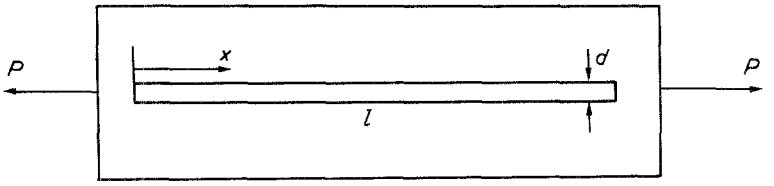

Figure 1 Composite monofibre model.

to σ_{rf} (Fig. 2d); therefore, the minimum length of the fragments will be $l_{cr}/2$.

In conclusion, the fibre will break into fragments of lengths between $l_{cr}/2$ and l_{cr}; i.e. the average value of l will be:

$$\bar{l} = 3l_{cr}/4 \quad (7)$$

The limit shear stress τ_l can be evaluated according to Equations 6 and 7 using the critical length obtained from the distribution of the fragment lengths, which gives $\bar{l}$. Actually, the fibre tensile strength (σ_{rf}) is not constant in each point because defects are randomly distributed along the fibre. Consequently, the experimental distribution of the fragment lengths is wider than in the case when σ_{rf} is constant along the fibre, because σ_{rf} values can differ from fragment to fragment. Thus, l_{cr} depends both on the mean value of σ_{rf} and on its distribution.

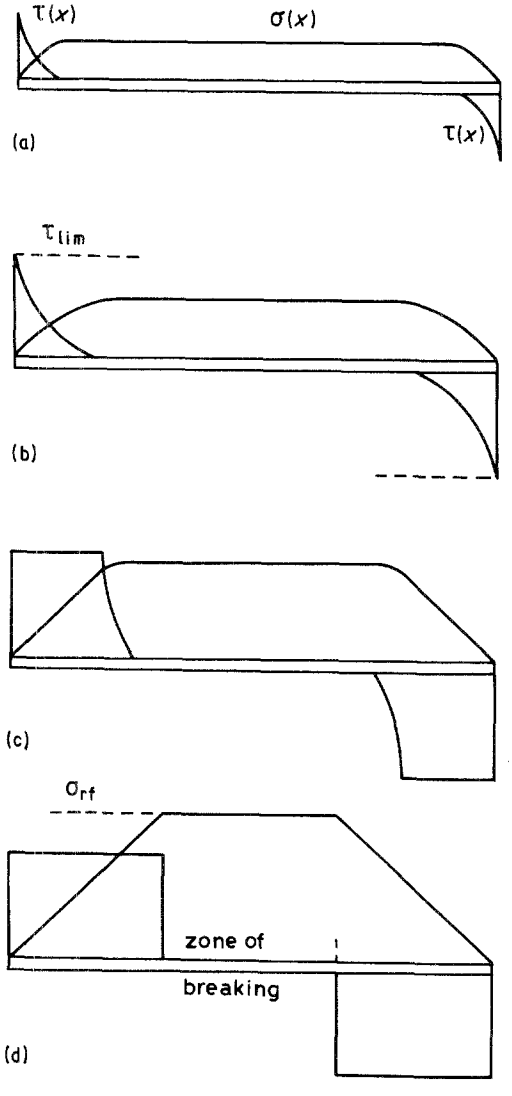

Figure 2 Stress distribution along a fibre: (a) very low load, (b) low load, (c) medium load, (d) high load.

3. Materials

High strength carbon fibres, Besfight HTA-7-6000, Toho Rayon Co., were used. Fibres were thoroughly washed in toluene at room temperature and dried. Single fibres, 7 μm diameter, were taken out of yarns and used to prepare the composites. Polyethersulphone (PES-300 P, I.C.I.) and Polyetherimide (ULTEM, General Electric Plastics) were characterized by us. The main properties of the two polymers and of the fibres are given in Table I.

4. Experimental details

4.1. Fibre characterization

All the mechanical tests were carried out in a thermostatic room at 23 $\mp$ 1° C and 50% r.h. Tensile tests were performed on monofilaments of different lengths (25, 50, 100 mm) at an elongation rate of 1 mm min^{-1} using an Instron 1175 dynamometer with a low load cell (full scale = 20 g) and elongation amplification ratio of 100 : 1. The mean curve is shown in Fig. 3. Average values of the properties are given in Table I. The large scatter in σ_r and ε_r in Table I is due to the defect distribution along the fibre. Defect distribution was examined on carbon monofilaments taken from the multifilament system as produced by Toho Rayon Co. Samples of useful length not too different from the average length of the fragments obtained by testing the composites (see later), were used. To obtain a good strength distribution, 100 specimens were tested.

Samples were prepared as follows: the ends of carbon monofilaments were glued using a polyester resin between two computer cards with the punched holes corresponding (Fig. 4). Specimens of useful length and equal to the width of the punched holes (1.4 mm), were obtained. Monofilaments were tested at an elongation

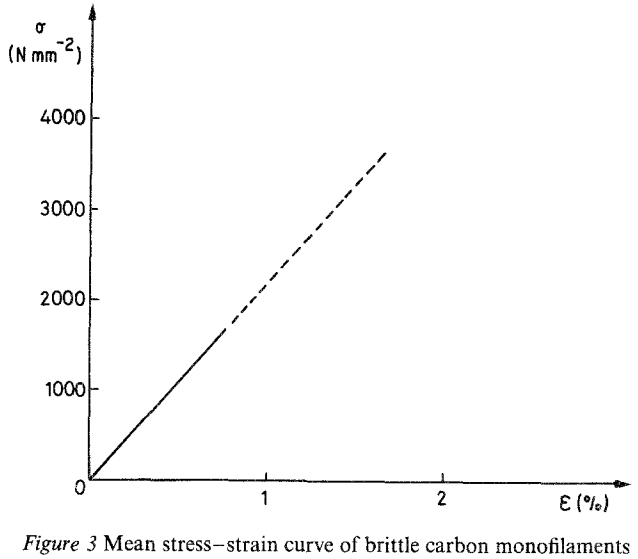

Figure 3 Mean stress–strain curve of brittle carbon monofilaments used in this work. The dotted part shows the interval of σ_r, ε_r between the minimum and the maximum values.

TABLE I Properties of materials at 23° C

Material	Mechanical properties						Other properties			
	Tensile tests (ASTM D638)				Shear tests ASTM D732					
	Elastic modulus,* 1% ($N\,mm^{-2}$)	Yield stress,* σ_y ($N\,mm^{-2}$)	Elongation at yield,* ε_y (%)	Poisson ratio, ν	Yield stress,* τ_y	Failure stress* τ_r	Density ($g\,cm^{-3}$)	T_g† (° C)	Linear dilatation coefficient, α_m [2] ($°C^{-1}$)	Radial stress on carbon filament due to thermal shrinkage ($N\,mm^{-2}$)
ULTEM	3090 (4.7%)	99.6 (2.4%)	5.7 (6.8%)	0.31 ± 0.02	37.0 (2.2%)	51.5 (5.5%)	1.23	214	5.6E-5‡	19.2
PES	2450 (2.6%)	80.8 (0.4%)	5.6 (3.9%)	0.31 ± 0.02	26.9 (2.4%)	37.7 (8.0%)	1.38	225.5	5.5E-5§	15.2
	Elastic modulus ($KN\,mm^{-2}$)	Failure stress, σ_r ($N\,mm^{-2}$)	Elongation at break, ε_r (%)	Elastic modulus, transverse [10] ($KN\,mm^{-2}$)			Density ($g\,cm^{-3}$)	Thermal dilatation coefficient ($°C^{-1}$) [10]		
								Longitudinal		Transverse
Carbon monofilaments	219 (6.4%)	1700 – 3800	0.8 – 1.7	16			1.77	−0.5 E-6		5.5 E-6

*Standard deviation in parentheses.
†DSC analysis
‡Technical bulletin from General Electric Plastics.
§Technical bulletin from I.C.I.

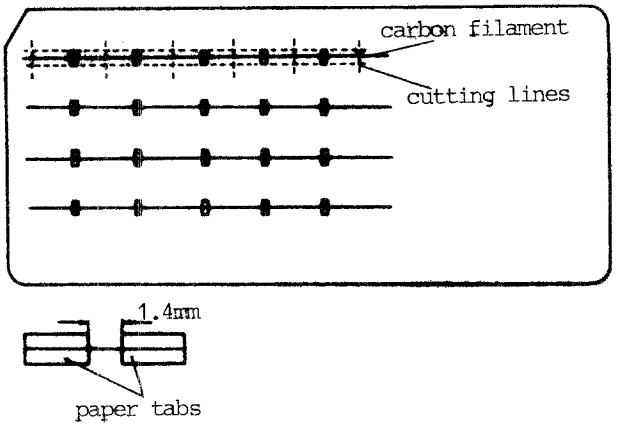

Figure 4 Short filaments assembly for the tensile tests.

rate of 1 mm min^{-1} using a low load cell (full scale 100 g).

Density was measured using a Westphal hydrostatic balance and long fibres.

The surface state of the fibres was examined by X-ray photoelectron spectroscopy (XPS), which gives information on the surface atomic composition (thickness $\simeq$ 3 nm). The main results are given in Table II. Samples A were analysed as-received, while samples B were thoroughly washed in toluene before analysis. A remarkable presence of oxygen (17 to 18%) in comparison with carbon (82 to 83% atomic) can be noticed. The asymmetric peak of carbon was approximated by two gaussian curves corresponding to the two different kinds of carbon C_I and C_{II}, respectively endowed with a binding energy of 284.6 eV attributed to hydrocarbon-bonded carbon and of 286.4 + 0.2 eV attributed to >C–OH (or >C=O). It can be noticed that the O/C_{II} ratio approximates unity. The ratio between the intensity of the photoemission peaks. O1s/C1s, is about 0.7; this value is similar to that found by other authors for highly oxidated fibres [4].

Fourier transform–infrared spectroscopy was used to analyse a film obtained from the coating on the carbon fibre by evaporation of a toluene solution: it was an epoxy resin.

4.2. Matrix characterization

Tests on matrices were carried out on materials moulded by compression moulding at 350° C at a pressure of 35 kg cm^{-2}. The tensile properties (yield stress, σ_γ and strain, ε_γ) were measured according to ASTM D 638 at an elongation rate of 1 mm min^{-1} (Fig. 5).

The elastic moduli, E, were obtained using a strain transducer with an amplification ratio of 125 : 1. The

TABLE II

	O (at %)	C_{tot} (at %)	C_I (at %)	C_{II} (at %)	I_o/I_c
A1	16.8	83.2	62.9	20.3	0.62
A2	18.7	81.3	57.6	23.7	0.71
B1	17.3	82.7	63.2	19.5	0.64
B2	18.3	81.7	59.7	22.0	0.69

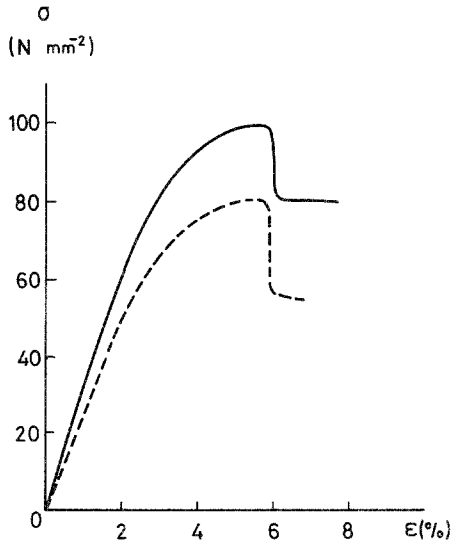

Figure 5 Tensile stress–strain curves of (---) PES and (——) ULTEM.

Poisson ratios, ν, were found using a transverse and longitudinal strain transducer MTI-DSST-II BI.

The shear yield stress and shear strength were measured by the punch tool shear test (ASTM D 732). Fig. 6 shows the stress–penetration curves. Densities were obtained using a Westphal hydrostatic balance.

4.3. Preparation of the composite samples

Sheets of about 0.5 mm thickness of ULTEM and PES were prepared by compression moulding at 350° C and 35 kg cm^{-2} pressure for 10 min. Different straight carbon filaments were interposed between two pre-moulded sheets which were subsequently pressed at 300° C and 90 kg cm^{-2}. The moulding temperature was kept lower than in the previous moulding to avoid polymer flow at the mould borders in order to prevent movement of the carbon filaments. Rectangular specimens (5 mm × 0.5 mm × 60 mm) were obtained by cutting with a dime and strained up to an elongation larger than the fibre breaking elongation. The fragment lengths were measured optically using a microscope because the polymers examined are amorphous and transparent.

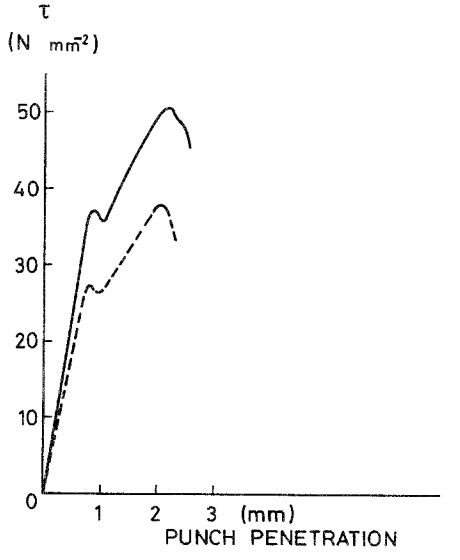

Figure 6 Shear stress–penetration curves of (---) PES and (——) ULTEM.

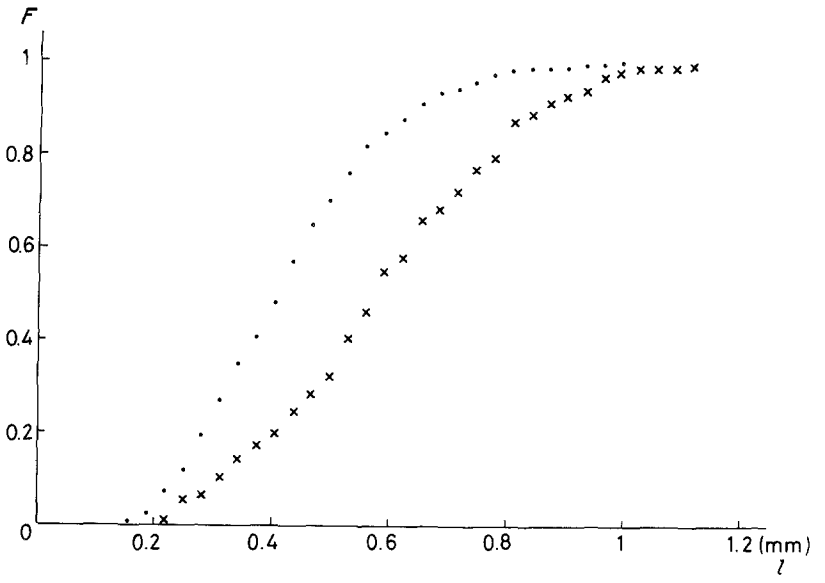

Figure 7 Probability distributions $F(l)$ of the lengths of carbon fibre fragments in the composites with (×) PES or (●) ULTEM.

The fibre breaking points were easily recognized by keeping the samples under load during the examination at magnifications of × 100 to × 200. Polarized light and a nonius were used. The sudden stress variation at the fragment ends caused a sharp birefringent effect in the matrix. In this way, by doing different tests, the lengths of 364 fragments immersed in ULTEM samples and those of 126 fragments immersed in PES, were measured.

5. Results and discussion

The experimental cumulative distribution functions $F(l)$ of the fragment lengths of PES and of ULTEM are illustrated in Fig. 7. $F(l)$ is the ratio between the number of fragments of length less than l and the total fragment number. The cumulative distribution function, $P_n(\sigma)$, represents the numerical fraction of monofilaments having a strength less than σ (Fig. 8). $P_n(\sigma)$ is the probability of a monofilament having a length of 1.4 mm being broken at a stress lower than or equal to σ.

The tensile strength of brittle fibres, as the carbon fibres, behaves according to the chain model proposed by Weibull [5]. Assume that we have a chain consisting of n links. If we know, through experimental measurements, the failure probability $P(\sigma)$ at any stress σ applied to "a single" link and if we want to determine the probability of failure P_n of the whole chain, we have to take into account the fact that the chain fails when one of the links fails. Consequently, the non-failure probability of the chain $(1 - P_n(\sigma))$ is equal to the probability of the simultaneous non-failure of all the links, i.e.

$$[1 - P_n(\sigma)] = [1 - P(\sigma)]^n \quad (8)$$

$P(\sigma)$ is the cumulative distribution function of one typical link of the chain: $P(\sigma)$ represents the probability that the typical link may have a tensile strength lower than σ.

Any distribution function can be written in the form:

$$P(\sigma) = 1 - e^{-\varphi(\sigma)} \quad (9)$$

This formulation has the advantage that the probability of a chain of n links surviving, $1 - P_n(\sigma)$, is very simply expressed by:

$$1 - P_n(\sigma) = [1 - P(\sigma)]^n = e^{-n\varphi(\sigma)}$$

from which

$$P_n(\sigma) = 1 - e^{-n\varphi(\sigma)} \quad (10)$$

The only necessary conditions the function $\varphi(\sigma)$ has to satisfy, are: to be positive, non-decreasing and vanishing at a value which is not necessarily equal to 0. The simplest function meeting these conditions is:

$$\varphi(\sigma) = \left(\frac{\sigma - \sigma_P}{\sigma_0}\right)^m \quad (11)$$

By introducing Equation 11 into Equation 10 we obtain:

$$P_n(\sigma) = 1 - e^{-n}\left(\frac{\sigma - \sigma_P}{\sigma_0}\right)^m \quad (12)$$

where σ_P and σ_0 are, respectively, the minimum and maximum values of the tensile strength, n is the number of ideal links in the chain, and m is a parameter. This equation is merely empirical and is valid as far as it fits the experimental observations. We observe that according to Equation 12 for $\sigma \leqslant \sigma_P$, $P_n(\sigma) = 0$ and for $\sigma = \sigma_0$, $P_n(\sigma)$ is not necessarily equal to 1 because fibres endowed with surviving capacity higher than σ_0 can exist. We calculated from the data of Fig. 8 the best values of the parameters σ_0, σ_P, n and m to obtain best agreement with the experimental results, by using a non-linear, optimization method [6]. The values: $\sigma_P = 1.21\ E - 4 \simeq 0\,\mathrm{N\,mm^{-2}}$, $\sigma_0 = 8440\,\mathrm{N\,mm^{-2}}$, $n = 13.3$, $m = 4.8$, were obtained for the carbon monofilaments. Therefore, our monofilaments can be ideally compared with links having a length of 1.4/13.3 = 0.105 mm. For composites, the average length of the carbon fragments, $\bar{l}$, (corresponding to a cumulative probability $F(l) = 0.5$) is found (looking at Fig. 7) to be 0.41 mm for the ULTEM–fibre system and 0.57 mm for the PES–fibre system.

The average l_{cr}, defined as $\bar{l}_{cr} = (4/3)\,\bar{l}$ (Equation 7) are: $\bar{l}_{cr}$ (ULTEM) = 0.55 mm; $\bar{l}_{cr}$ (PES) = 0.76 mm; therefore, the corresponding numbers of links are, respectively, 5.24 and 7.24. According to Equation 12 it is possible to calculate $P_{5.24}(\sigma)$ and $P_{7.24}(\sigma)$ which have to be used for our systems.

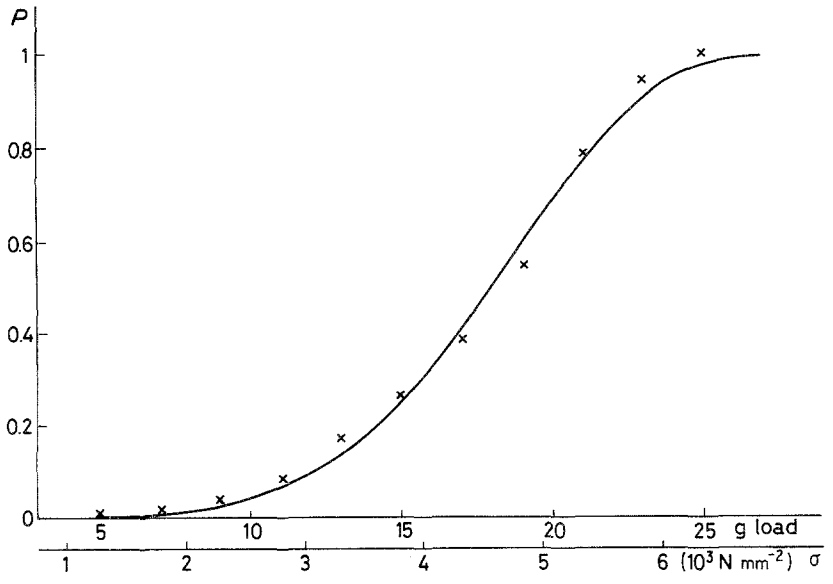

Figure 8 Probability strength distribution $P(\sigma)$ of carbon filaments (l = 1.4 mm). (×) Experimental data, (——) theoretical curve.

The average strength of a monofilament consisting of n ideal links is given by [2]:

$$\bar{\sigma}_{rf} = \int_{\sigma_P}^{\infty} \sigma \frac{dP_n(\sigma)}{d\sigma} d\sigma = \sigma_P + \frac{\sigma_0}{n^{1/m}} \Gamma\left(\frac{m+1}{m}\right) \quad (13)$$

where Γ is the complete Gamma function whose value in our case is 0.9164 [7]. Equation 13, which is not presented in the literature, is worked out in the Appendix.

In this way $\bar{\sigma}_{rf}$ is calculated at a length corresponding to $\bar{l}_{cr}$ using for n in Equation 13 the number of links (5.24 and 7.24) found on the basis of the critical lengths. We obtain $\bar{\sigma}_{rf}$(ULTEM) = 5500 N mm^{-2}; $\bar{\sigma}_{rf}$(PES) = 5100 N mm^{-2}. By means of Equation 5 we calculate: τ_l(ULTEM) = 35 N mm^{-2}, and τ_l(PES) = 23.5 N mm^{-2}.

Adhesion is the result of very complex phenomena. In the absence of chemical bonds between fibre and matrix, adhesion is attributed to the Van der Waal's interactions, which are more effective when the average distances between the atoms of the two phases are small: the differential thermal shrinkage of the two materials gives rise, at the interface, to a pressure which increases the Vander Waal's forces. When an external load is applied the shear slipping between the two phases is prevented until the shear stress $\tau = \mu P$ reaches a limiting value (τ_l); μ represents the friction coefficient which encompasses in an empirical factor all the chemical–physical interactions. This equation was proposed by Outwater [8].

For a single cylindrical inclusion, P is expressed by the equation [9]:

$$P = \frac{(\bar{\alpha}_m - \bar{\alpha}_f)\Delta T E_m}{(1 + \nu_m) + (1 - \nu_f)E_m/E_f} \quad (14)$$

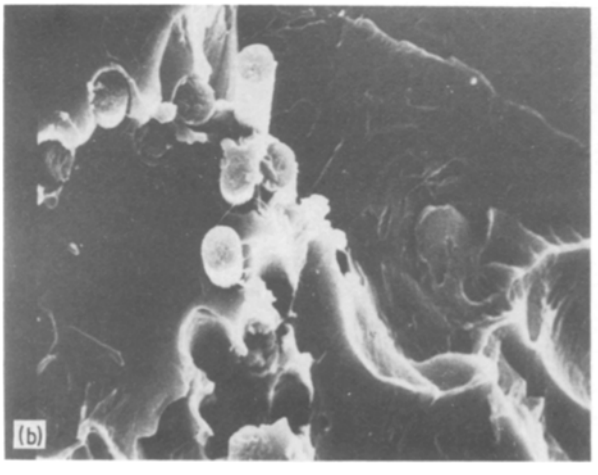

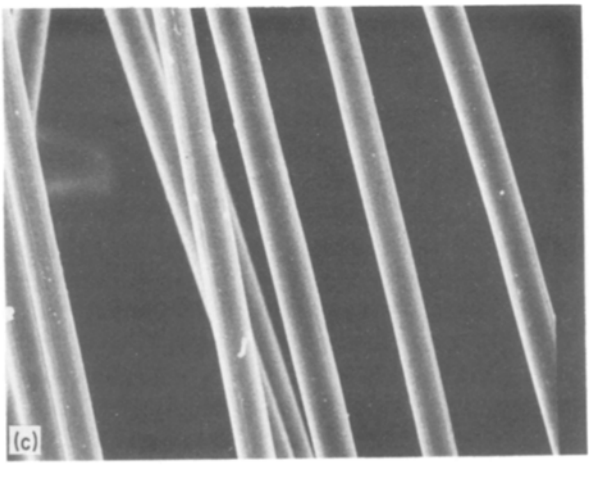

Figure 9 Electron scanning micrographs of the fracture surfaces of: (a) ULTEM–fibres, (b) PES–fibres composites; (c) carbon fibres after extraction with toluene. × 750.

Equation 6 represents the shear stress, τ_l, evaluated on the basis of the experimental l_{cr}, which operates at the interface when failure occurs. This equation has a phenomenological character and it is not useful in predicting the reason for the failure mechanism.

On the other hand, microscopic examination of the fibre surface can give useful information. The presence of polymer adhering to the surface shows that interfacial adhesion stronger than the matrix strength exists. In the case of our materials there is no evidence of a chemical bond between carbon fibre and polymer; only Van der Waal's interactions are expected, because the carbon surface is highly oxidized and the polyethersulphone and polyetherimide macromolecules have polar groups. This is confirmed by the fact that no matrix material can be seen on the fibres which are bare (Fig. 9).

τ_l values cannot be greater than the yielding shear stress of the matrix. Our experimental data show that τ_l has a value close to the matrix shear yield stress, τ_y, for the ULTEM–fibre system. In the case of PES matrix, τ_l is slightly lower than τ_y (Table I). We attribute this different behaviour both to the different values of pressure due to the differential thermal shrinkage, and to the different chemical nature of the matrices. Table I shows the values of pressure (P) for the materials which are consistent with the experimental τ_l values. Radial stresses ($\sigma_r^t = P$) due to thermal effects calculated according to the room temperature elastic moduli considering a temperature range between glass transition and room temperature.

The carbon fibre properties used in the calculations are those measured in the transverse direction (Table I).

The experimental friction coefficients calculated according to $\mu = \tau_l/\sigma_r^t$ are $\mu = 1.92$ for the ULTEM–fibre system and $\mu = 1.55$ for the PES–fibre system.

We conclude that adhesion is efficient with both matrices, and that the shrinkage phenomena are most important because of the high glass transition temperatures (softening) of the thermoplastics studied.

Acknowledgements

We thank Dr F. Garbassi (Inst. Donegani-Montedison) for his contribution to this work which was partially supported by Progetto Finalizzato Energetica II (C.N.R.) and Ministero della Pubblica Istruzione.

Appendix

$$\bar{\sigma} = \int_{\sigma_P}^{\infty} \sigma \frac{dP_n(\sigma)}{d\sigma} d\sigma \quad (A1)$$

$$P_n(\sigma) = 1 - e^{-n(\sigma-\sigma_P/\sigma_0)^m} \quad (A2)$$

Deriving Equation A2

$$\frac{dP_n(\sigma)}{d\sigma} = [-e^{-n(\sigma-\sigma_P/\sigma_0)^m}]\left[-nm\left(\frac{\sigma-\sigma_P}{\sigma_0}\right)^{m-1}\frac{1}{\sigma_0}\right]$$

$$= \frac{nm}{\sigma_0}\left(\frac{\sigma-\sigma_P}{\sigma_0}\right)^{m-1} e^{-n(\sigma-\sigma_P/\sigma_0)^m} \quad (A3)$$

Introducing Equation A3 into Equation A1:

$$\bar{\sigma} = nm\int_{\sigma_P}^{\infty}\frac{\sigma}{\sigma_0}\left(\frac{\sigma-\sigma_P}{\sigma_0}\right)^{m-1} e^{-n(\sigma-\sigma_P/\sigma_0)^m} d\sigma \quad (A4)$$

With the following substitutions:

$$\left(\frac{\sigma-\sigma_P}{\sigma_0}\right)^m = t \quad (A5)$$

$$dt = m\left(\frac{\sigma-\sigma_P}{\sigma_0}\right)^{m-1}\frac{d\sigma}{\sigma_0} \quad (A6)$$

$$\frac{\sigma-\sigma_P}{\sigma_0} = t^{1/m} \quad (A7)$$

$$\sigma = \sigma_0 t^{1/m} + \sigma_P \quad (A8)$$

we get

$$\bar{\sigma} = n\int_{t(\sigma_P)}^{t(\infty)}(\sigma_0 t^{1/m} + \sigma_P)e^{-nt} dt \quad (A9)$$

$$\bar{\sigma} = n\sigma_P\left[\frac{e^{-nt}}{-n}\right]_{t(\sigma_P)}^{t(\infty)} + n\int_{t(\sigma_P)}^{t(\infty)}\sigma_0 t^{1/m}e^{-nt} dt \quad (A10)$$

$$\sigma = \sigma_P \rightarrow t = 0 \quad (A11)$$

$$\sigma = \infty \rightarrow t = \infty$$

$$\bar{\sigma} = \sigma_P + n\int_0^{\infty}\sigma_0 t^{1/m}e^{-nt} dt \quad (A12)$$

Substituting

$$1/m = z - 1 \Rightarrow z = \frac{m+1}{m} \quad (A13)$$

into Equation A12:

$$\bar{\sigma} = \sigma_P + n\int_0^{\infty}\sigma_0 t^{z-1} e^{-nt} dt$$

$$= \sigma_P + \sigma_0\frac{n^z}{n^{z-1}}\int_0^{\infty} t^{z-1} e^{-nt} dt \quad (A14)$$

$$n^z\int_0^{\infty} t^{z-1} e^{-Kt} dt = \Gamma(z) \quad [7] \quad (A15)$$

$$\bar{\sigma} = \sigma_P + \frac{\sigma_0}{n^{z-1}}\Gamma(z) \quad (A16)$$

$$\bar{\sigma} = \sigma_P + \frac{\sigma_0}{n^{1/m}}\Gamma\left(\frac{m+1}{m}\right) \quad (A17)$$

References

1. A. T. DIBENEDETTO and L. NICOLAIS, *Plast* **5** (1979) 83.
2. M. MIWA, T. OHSAWA and K. TAHARA, *J. Appl. Polym. Sci.* **25** (1980) 795.
3. A. KELLY, "Strong Solids" (Clarendon Press, Oxford, 1973).
4. T. TAKAHASI and A. ISHITANI, *Carbon* **22** (1984) 43.
5. W. WEIBULL, *J. Appl. Mech. ASME* **18** (1951) 293.
6. G. BUZZI FERRARIS, *Ingegnere Chimico Italiano* **4** (1968) 171.
7. M. ABRAMOWITZ and I. A. STEGUN, "Handbook of Mathematical Functions" (Dover, New York, 1965).
8. J. O. OUTWATER Jr, *Mod. Plast.* **33** (1956) 156.
9. G. GERARD and A. C. GILBERT, *J. Appl. Mech.* ASME **24** (1957) 355.
10. G. NIEDERSTADT, Kunstsoffe **74** (1984) 686.

Received 20 June
and accepted 9 September 1986